Concentration dependence of the adsorption of metal-free tetra(4-carboxyphenyl) porphyrin (TCPP) on Hexagonal Boron Nitride

Anne-Charlotte Nellissen[a], Yuanzhi Xia[a], Tianze Hu[a], Jonathan B.F. Vandenwijngaerden[a], Eduard Fron[a], Steven De Feyter[a], Stijn F. L. Mertens[b,*], Mark Van der Auweraer[a,*]

AFFILIATIONS

[a]Laboratory for Photochemistry and Spectroscopy, KU Leuven (Chem & Tech, Celestijnenlaan 200F, 3001 Leuven, Belgium)

[b]Chemistry Department and Energy Lancaster, Lancaster University (LA1 4YB Lancaster, United Kingdom)

*Corresponding authors: s.mertens@lancaster.ac.uk or stmerten@gmail.com & mark.vanderauweraer@kuleuven.be

KEYWORDS

Dye aggregation, porphyrins, hexagonal boron nitride, energy transfer, nanocrystals, adsorption

ABSTRACT

The adsorption and self-assembly of metal-free tetra(4-carboxyphenyl) porphyrin (TCPP) from ethanol on the surface of hexagonal boron nitride (hBN) was studied to determine the influence of the concentration of the solution on the self-assembly/aggregation and spectroscopic properties of the adsorbed TCPP. The adsorption isotherm indicates that at saturation the TCPP molecules adsorb edge-on with the macrocycle nearly perpendicular parallel to the hBN surface. On the other hand, the atomic force (microscopy AFM) micrographs indicate that a monolayer of flat-on adsorbed TCPP molecules, observed for adsorption from a diluted

solution transforms into edge-on adsorbed molecules when more concentrated solutions are used. While for adsorption from a dilute solution, the stationary emission spectra correspond to those reported in literature, they shift 15 nm to longer wavelengths when adsorption occurs from more concentrated solutions suggesting stronger interaction between neighboring chromophores for edge on adsorption. The latter is also suggested by a broadening of the red edge of the fluorescence excitation spectra. Fluorescence decays obtained for the different emission wavelengths can be analyzed globally as quadruple exponential decays linking the four decay times. The non-mono-exponential character of the decay is attributed mainly to energy transfer to non-fluorescent traps. The longest decay time decreases from 5.9 ns for the sample prepared by adsorption from a dilute solution to 4.6 and 4.0 ns from samples prepared from more concentrated solutions. These decay times are about 50 % shorter than the fluorescence decay time of TCPP in ethanol.

INTRODUCTION

In the last decade hexagonal boron nitride (hBN) gained interest as a platform to study the adsorption of molecules and the corresponding photophysics. hBN is iso-structural to graphene with a hexagonal lattice arrangement consisting of alternating boron and nitrogen atoms in a sp^2 hybridization. hBN can form multilayers where the individual layers stick together by van der Waals interactions (AB-stacking). Furthermore, hBN is a thermally and chemically stable material with insulating properties (the indirect bandgap amounts to 5.95 eV).[1-4]

Different molecules can adsorb to the surface of hBN nanosheets and the corresponding nanomesh structures.[5-14] This physisorption is driven by van der Waals interactions, interactions with π-electrons of the basal plane and electrostatic interactions with the polarized B-N bonds. The growth of n-alkane adsorption layers on hBN occurs via island formation, where n-alkanes adsorb with their principal axis parallel to each other or in a herringbone pattern as observed for n-alkanes on graphite.[9-12] Mixtures of n-alkanes with different chain

lengths phase separate on the hBN surface depending on their preference for parallel or herringbone adsorption.[5,6] Hexacontane ($C_{60}H_{122}$) forms lamellar rows with its molecular axis parallel to the zigzag direction of hBN as observed for longer alkanes on graphite.[15] The adsorption of several layers of N,N′-ditridecylperylene 3,4,9,10-tetracarboxylic diimide (PTCDI-C_{13}) on hBN by physical vapor deposition shows different adsorption behavior for the first and the second/third layer. The first layer adsorbs flat-on with a brick-wall arrangement and its spectroscopic properties suggest the formation of J-type aggregates. The second and third layer rather adsorb edge-on and the consequent side-by-side arrangement leads to the formation of H-type aggregates.[7] Cyanine dyes preferentially form monolayers of flat-on adsorbed molecules.[13,14] Polythiophene (PT) polymers form J-type aggregates when adsorbed from toluene on the surface of hBN. Its adsorption induces an increased planarization with interdigitation of the alkane chains of one PT molecule with those of neighboring PT backbones.[16]

The adsorption of tetra(4-carboxyphenyl)porphyrin (TCPP) molecules on several surfaces was already discussed in literature. TCPP molecules adsorbed from an ethanolic solution on a TiO_2 surface occupy 1.2 nm^2/molecule at saturation, which is intermediate between the area of flat-on adsorbed molecules (2.3 nm^2/molecule) and of standing TCPP molecules (edge-on adsorption) which would occupy an area of 0.6 nm^2/molecule.[17] This suggests an intermediate orientation of the adsorbed TCPP molecules, the formation of an incomplete layer of edge-on adsorbed molecules or the formation of multilayers of flat-on adsorbed molecules. In contrast to what happens on TiO_2, Korolkov *et al*.[8] observed that TCPP molecules dissolved in ethanol adsorb parallel to the surface (flat-on) on a hBN surface. Atomic force probe microscopy revealed a self-assembly forming square and hexagonal structures, which are stabilized via in-plane hydrogen bonding between neighboring TCPP molecules. To optimize van der Waals interactions with the substrate the TCPP molecules, where the aryl side groups cannot adopt a coplanar structure with the macrocycle, are distorted to a bowed geometry. This distortion also explains the red shifted fluorescence of the adsorbed TCPP molecules. When adsorbed

from respectively ethanol and dimethylformamide (DMF) on highly oriented pyrolytic graphite (HOPG) and MoS_2 TCPP only adsorbs flat-on and self-assembles in a square geometry.

Here we present a systematic study of the influence of the concentration of the solution on the morphology, stationary and time resolved spectroscopy of TCPP adsorbed on hBN. In this way we will try to investigate to what extent multilayer formation can occur and how the latter are organized.

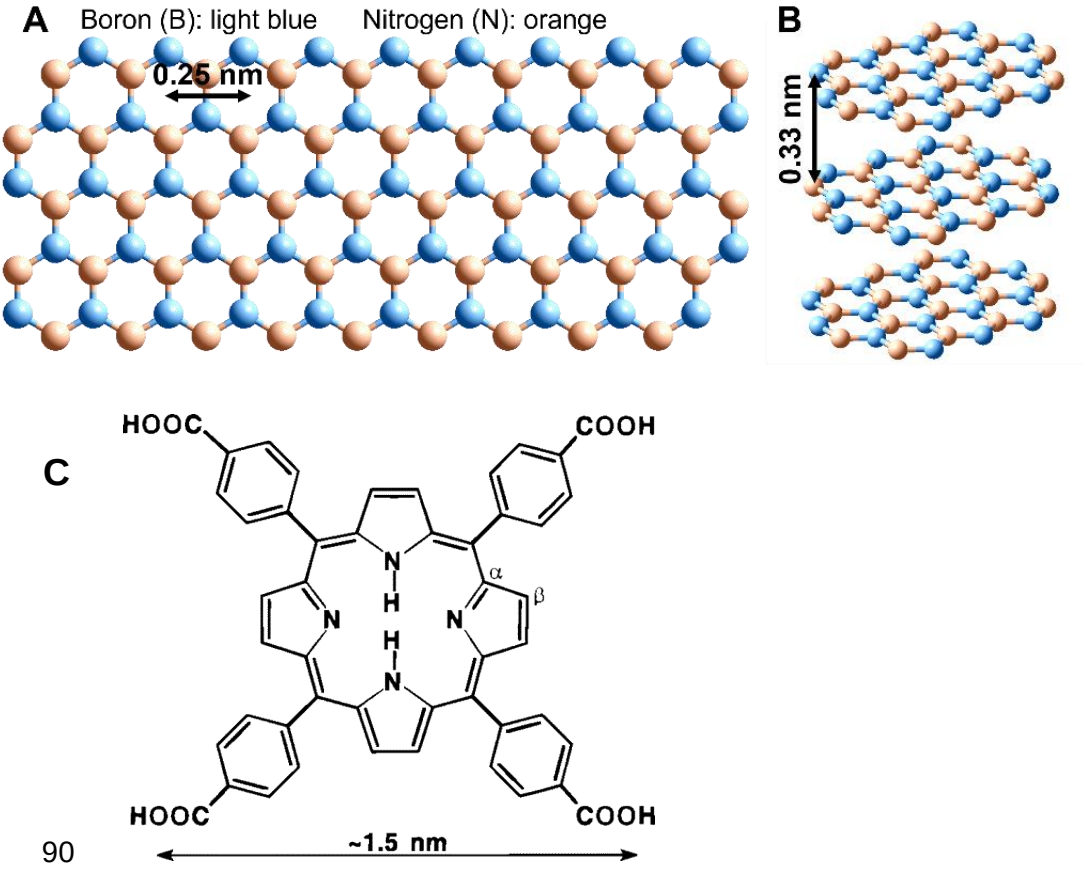

Figure 1 Monolayer hBN (A) and multilayer formation by hBN (B). General structure of TCPP molecule (C).

MATERIALS & METHODS

For the determination of the adsorption isotherm and the stationary and time-resolved spectroscopy hBN platelets (multilayers) with lateral size below 5 µm were acquired from Sigma-Aldrich and used without further treatment. The hBN crystals used for the AFM experiments are a gift from the research group of prof. Kenji Watanabe and prof. Takashi

Taniguchi of the National Institute of Materials Science (NIMS), Tsukuba, Japan. The flakes of hBN were transferred via mechanical exfoliation (scotch-tape method) on the silicon substrates which were cleaned as described in the SI.

The solvents ethanol (Merck, 99.9%), Milli-Q water (Merck, ultrapure), ethanol (Sigma-Aldrich, ultragrade) and n-heptane (Sigma-Aldrich, 99%) were used without further purification. Metalfree TCPP was purchased from TCI Chemicals and used without further treatment.

The preparation of the samples of TCPP in solution and adsorbed on hBN for determination of the molar extinction coefficient, adsorption isotherm, atomic force microscopy, steady-state spectroscopy and fluorescence decays are described in the SI.

The morphology of the TCPP:hBN:silicon samples was studied using atomic force microscopy (AFM) on a Cypher ES (Asylum Research) system at 32°C. The topography images were extracted using the tapping mode at the air/substrate interface using OMCL-AC240TS-R3 probes (Olympus Corporation, spring constant ~2 N/m, resonance frequency ~70 kHz) for blank measurements in absence of TCPP molecules and for samples where TCPP was adsorbed on hBN covered with the adsorbed porphyrin molecules. The same tip was used to locally scratch away the TCPP layer in the contact mode at a constant force of 100 nN to determine the thickness of the adsorbed dye layer. All AFM images were analyzed and processed using Scanning Probe Imaging Processor (SPIP 6.3.5) software from Image Metrology ApS.[13,18]

UV-visible absorption spectra of dilute solutions of TCPP in ethanol were recorded in quartz cuvettes with path length of 1 mm and 1 cm using a Perkin Elmer Lambda40 spectrophotometer for the construction of the adsorption isotherms and to study the potential aggregation of TCPP in ethanol. The absorption spectra were collected with blank corrections (pure solvent). The emission and excitation spectra of TCPP adsorbed on hBN were determined with a Horiba Jobin Yvon Fluorolog 3 spectrofluorometer in front-face configuration, while those of TCPP in solution were recorded in right-angle configuration. The excitation spectra were corrected for the wavelength dependence of the intensity of the

125 excitation light and for temporal fluctuations of this intensity. The emission spectra were
126 corrected for the wavelength dependence of the detection channel throughput and the
127 sensitivity of the detector.[13]

128 The fluorescence decays were determined by Time Correlated Single Photon Counting (TC-
129 SPC) technique.[19-22] The samples were excited by a Ti:Sapphire laser (Tsunami mode-locked,
130 model 3950, Spectra Physics) pumped by a diode-pumped CW laser (Millenia 10W, Spectra
131 Physics). The Tsunami output (800 nm, 2 ps, 82 MHz) passed through a pulse selector (Model
132 3980, Spectra Physics) to reduce its repetition rate down to 8.2 MHz and a frequency
133 doubler/tripler (GWU, Spectra Physics) to obtain 400 nm excitation pulses The fluorescence,
134 collected at right-angle, was spectrally resolved by a monochromator (Sciencetech 9030, slit
135 width 1 mm), and detected by a microchannel plate photomultiplier tube (MCP-PMT, R3809U-
136 51, Hamamatsu). A time-correlated single photon timing PC module (SPC 630, Becker &
137 Hickl) was used to obtain the fluorescence decay histogram in 4096 channels. The decays
138 were recorded with 10 000 counts in the peak channel, and a channel width of 50 ps per
139 channel. In this way, the time window amounted to 30 ns.

140 The decays were analysed with the time-resolved fluorescence analysis (TRFA) software,
141 which is based on the iterative reconvolution of a triple or quadruple-exponential decay)Eq.
142 1) with the instrumental response function (IRF).

$$I(t) = \sum_i A_i \exp\left(-\frac{t}{\tau_i}\right) \qquad \text{Eq. 1}$$

$$\langle\tau\rangle = \frac{\sum_i A_i \tau_i}{\sum_i A_i} \qquad \text{Eq. 2}$$

143 In equation 1, A_i and τ_i correspond to the amplitude and the decay time of the i^{th} component
144 of the decay. The average decay time $\langle\tau\rangle$ is then given by Eq. 2.[21] The goodness of fit was
145 determined by χ^2 and visual inspection of the residuals and their autocorrelation function. For
146 all samples except the fluorescence decay at 745 nm of the sample prepared by adsorption
147 from a 150 µM solution of TCPP, χ^2 was below 1.2.

In order to be able to compare decays of different samples or decays obtained at different emission wavelengths for the same sample, the amplitude of the different components will be expressed as a normalized amplitude α_i) (in %) in the tables.

$$\alpha_i = \frac{A_i}{\sum_i A_i} 100 \qquad \text{Eq. 3}$$

The contributions in % of each decay component, p_i, to the stationary emission spectrum are given by

$$p_i = \frac{A_i \tau_i}{\sum_i A_i \tau_i} 100 \qquad \text{Eq. 4}$$

In order to evaluate the influence of the emission wavelength on the features of the decays, the decays of the same sample obtained at emission wavelengths ranging from 653 to 745 nm were analyzed globally by linking three or four decay times. One should note however that there is no physical reason to have three or four components with a different decay time. Actually non-exponential and stretched exponential decays can as well be analyzed as a sum of exponentials.[14,23] Hence one should be careful when trying to associate the different components of the decay with specific excited species or to give a physical meaning to the different decay times and the corresponding amplitudes or their contribution to the stationary emission spectrum. For the results shown here such interpretation can only make sense for the component with the longest decay time, the component giving the largest contribution to the stationary emission and the average decay time $\langle\tau\rangle$.

RESULTS & DISCUSSION

Determination of the adsorption isotherm

Within the concentration range used for the adsorption of TCPP (1 µM to 600 µM) the absorption spectra of a solution of TCPP in ethanol (Figure S1 A) and the linearity of the Lambert Beer plot (Figure S2) show no indication for a limited solubility or aggregation of

TCPP in ethanol (see SI). The absence of aggregation can be attributed to steric hinder induced by the nonplanar orientation of phenyl rings attached to the porphyrin core.

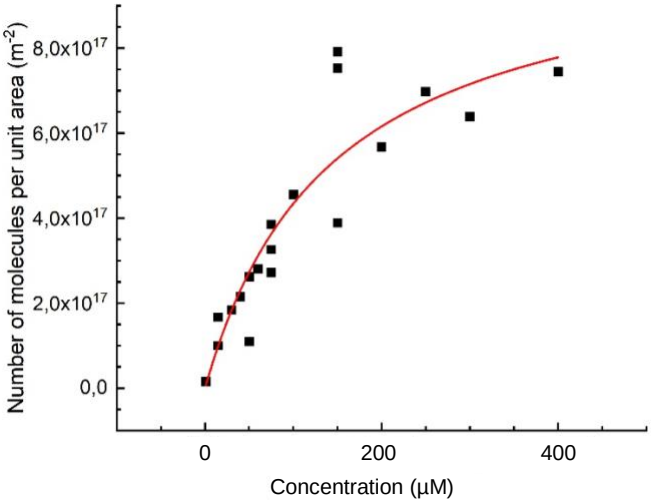

Figure 2 Adsorption isotherm of TCPP on hBN from an ethanol solution of TCPP. The data were fitted to a Langmuir isotherm.

The molar extinction coefficient (ε) of TCPP in ethanol was obtained using the same procedure as used for adsorption of thiacarbocyanine dyes on hBN.[13] For the determination of the adsorption isotherm 10 mg of hBN powder was dispersed in 4 mL of the dye solution (further called initial solution) and transferred to conical flacons. The dispersion was centrifuged for 1 hour at 4000 rpm. The difference in absorbance (at 417 nm) between the TCPP solution before hBN addition and of the supernatant after the addition of hBN and centrifugation (see SI) combined with the molar extinction coefficient at 417 nm allowed us to determine the change in concentration of the TCPP solution by adsorption on hBN and hence the number of TCPP molecules that are adsorbed on the surface of 10 mg hBN after the addition of hBN to the initial dye solution (details see SI). This approach has the drawback that at higher concentrations the relative error on this difference becomes quite significant. Therefore, no results are given for concentrations above 400 µM. Combining these data with the specific surface area of 11 ± 2 m^2/g of the hBN platelets[13] allowed us to plot the number of immobilized

adsorbed TCPP molecules per unit area versus the initial dye concentration rendering the adsorption isotherm of TCPP on hBN (Figure 2). The adsorption isotherm could be fitted to the Langmuir-isotherm.[24]

$$Q_e = Q_{Sat} \frac{K_{La} c}{1+K_{La} c} \qquad \text{Eq. 5}$$

In Eq. 5 Q_e is the number of molecules adsorbed on the surface of hBN per unit area at equilibrium (surface density), Q_{Sat} is the number of adsorbed molecules per unit area on the hBN surface at saturation, c is the initial adsorbate concentration in solution, and K_{La} is the affinity constant for adsorption.

Table 1: Data obtained by fitting the adsorption of TCPP on hBN to a Langmuir isotherm. R^2 is the correlation coefficient.

	Q_{Sat} (molecules/m^2)	K_{La} (M^{-1})	R^2
TCPP	1.05±0.17x10^{18}	6.5±2.4x10^3	0.83

At saturation, Q_{Sat} amounts to 1.05 ± 0.17 x 10^{18} adsorbed molecules/m^2 which corresponds to an area of 0.95 ± 0.15 nm^2/molecule. This value is much smaller than the value reported[17] for a flat-on adsorption (2.3 nm^2/molecule or 4.3 x 10^{17} molecules/m^2) and even smaller than the value of 1.2 nm^2/molecule at saturation (corresponding to a saturation density Q_{Sat} of 8.3 x 10^{17} molecules/m^2) reported by Cherian *et al.*[17] for TCPP adsorbed on TiO_2. It is somewhat larger than the value of 0.6 nm²/ molecule that can be expected for edge on adsorption. This suggests that TCPP adsorbs nearly edge on, in contradiction with the work of Korolkov *et al.*[8] who found a nearly flat-on adsorption of TCPP on hBN from scanning probe microscopy experiments. One should note that these large densities of adsorbed TCPP are only obtained (Figure 2) at concentrations of TCPP above 200 µM, i.e. about 15 times higher than the concentration of TCPP used by Korolkov *et al.*.[8] This suggests that the adsorption changes from flat-on to edge-on as increasing the concentration of TCPP. In the next section this

assumption will be tested using AFM. The value of K_{La} (Table 1) is five to ten times lower than the values obtained for the adsorption of cyanine dyes on hBN (3.0×10^4 M^{-1} to 1.1×10^5 M^{-1}) although the area of TCPP is about twice that of a molecule of the cyanine dyes. Even if one considers that the values of K_{La} are underestimated by a factor of two due the smaller values of Q_{sat} relevant for lower concentrations K_{La} remains still two to five times smaller than the values found for the adsorption of cyanine dyes on hBN. This could be due to the non-coplanar orientation of the phenyl rings compared to the porphyrin core, which will lead to a smaller interaction between the porphyrin π-cloud and hBN or to deformation of hBN to optimize the interaction of the porphyrin core with hBN.[8,10]

Atomic force microscopy

The preparation protocol shown in the SI allowed to prepare large flakes (20-50 µm) of hBN with a clean and flat surface, as depicted earlier[13,15], which are suitable to visualize the on-surface changes in topography upon adsorption of TCPP.

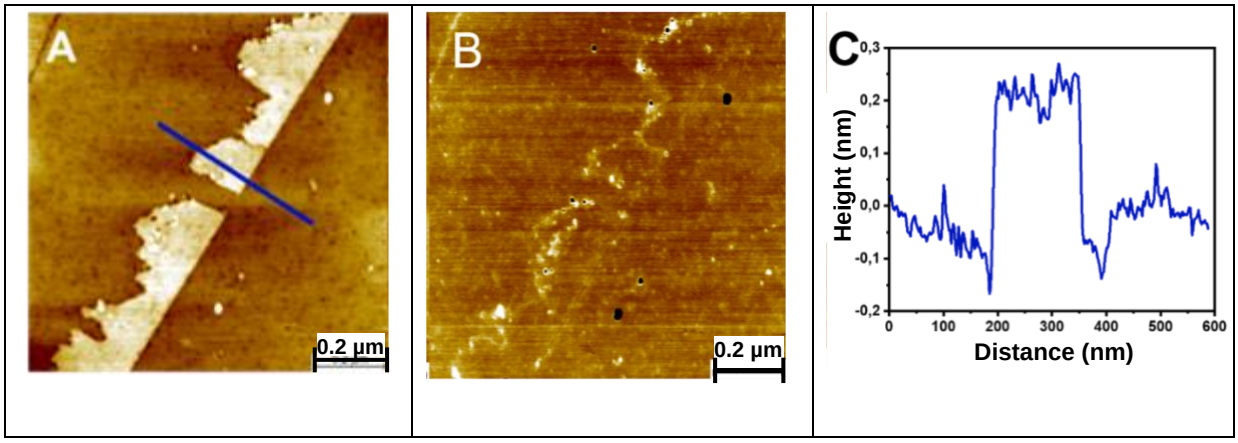

Figure 3 Topographic (A) and phase (B) AFM image of TCPP:hBN adsorbed from a 13 µM TCPP solution in ethanol. C: Line profile along the blue line in Figure 3 A.

In the topography images the AFM micrographs of TCPP adsorbed on hBN from its ethanolic solution with an initial concentration of 13 µM showed a surface with holes (dark brown) and locally covered by higher patches (whitish color in Figure 3 A) with a thickness of 0.3 ± 0.1 nm (Figure 3 C). The corresponding phase images (Figure 3 B) showed no phase difference

between the patches on top of the layer and the layer suggesting that the patches have the same identity (TCPP) as the layer underneath. Also, the thickness of the patch (0.3 ± 1 nm) corresponds to that of an aromatic molecule, (0.30 to 0.34 nm), suggesting the patch is just the onset of the adsorption of a second layer. A root-mean-square (RMS) analysis of the height, performed to identify the uniformity of the layer, yielded an RMS value of 0.06 nm. This value suggests a high uniformity of the observed surfaces. In order to get information on the thickness of the underlying layer, a 0.2x0.2 µm local square was scratched away (Figure 4 A and B) in contact mode. A height histogram of the scratched area and its surroundings shows a bimodal distribution with the green and orange maxima corresponding to respectively the height of the scratched area and the undisturbed part of the sample surroundings. The distance between the maxima amounts to 0.24 ± 0.1 nm (Figure 4 C), which is close to the values reported in literature[8] for the thickness of a TCPP layer adsorbed on hBN. This confirms the monolayer nature of major part of the adsorbed TCPP layer as well as a flat-on adsorption of TCPP. Although according to Korolkov *et al*.[8] in-plane hydrogen bonding between adsorbed neighboring TCPP molecules should lead to self-assembly in a square or hexagonal geometry, this could not be observed here as it was not possible to obtain molecular resolution.

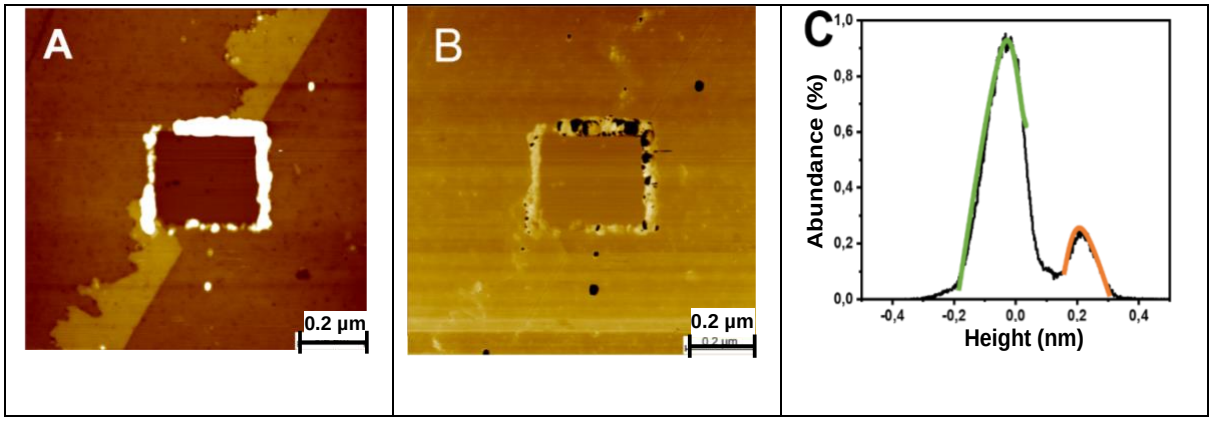

Figure 4 Topographic (A) and phase (B) AFM image of the scratched area and its surroundings for TCPP:hBN adsorbed from a 13 µM TCPP solution in ethanol. Height histogram (C) of the scratched area and its surroundings.

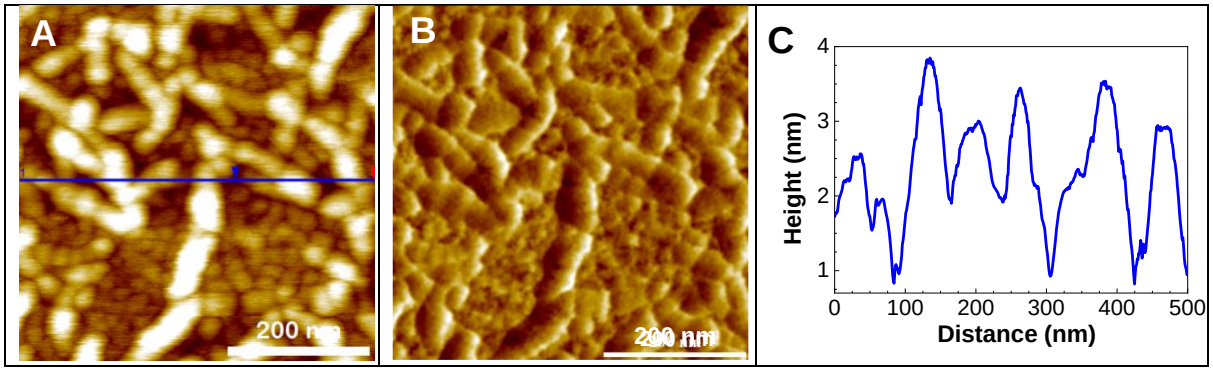

Figure *5* Topographic (A) and phase (B) AFM image of TCPP:hBN adsorbed from a 75 µM TCPP solution in ethanol. C: The line profile along the blue line in Figure 5 A.

For TCPP adsorbed from a more concentrated solution (75 µM), the topography image shows that part of the surface is covered by elongated structures with a length of 50 to 200 nm and a width of about 25 ± 5 nm (Figure 5 A). The same structures can be observed in the phase image (Figure 5 B). The line profile along the blue line (Figure 5 C) shows that the height varies most often in steps of 1.2 ± 0.2 nm although also steps of 2.4 or 2.7 nm are observed. This is much larger than the thickness of a molecule of TCPP and rather matches its diameter of about 1.5 nm. Adsorption from a 150 µM and a 450 µM solution leads to structures of similar height and width (Figure S4 and S5) although they get a more fibrous morphology. Such structures can correspond to single and double layers of edge on adsorbed TCPP molecules having a diameter of about 1.5 nm (Figure 1 C). From the images it cannot be deduced whether there is an underlying layer of flat on adsorbed molecules as observed for adsorption from a 13 µM solution. The transformation from a packing close to flat on absorption (occupying an area of 2.3 nm²/molecule) to edge on adsorption (occupying an area of 0.6 nm²) upon increasing the concentration can be explained by the thermodynamics of the adsorption process.[25] The foot print of an edge on adsorbed molecule of TCPP (0.6 nm²) is still smaller than the available area per adsorbed molecule at the saturation of the adsorption isotherm (0.95 ± 0.15 nm²/molecule). This discrepancy can be explained by a partial coverage of the substratum by adsorbed TCPP (see Figure 5 A and 5 B). As the AFM images suggest a drastically different packing and corresponding intermolecular distances when adsorption occurs from more concentrated solutions this difference should also be observable in the

electronic absorption and fluorescence spectrum considering the distance dependence of exciton interaction[26-28]

Spectroscopy of TCPP adsorbed on hBN from a 15 µM solution

The electronic spectra of porphyrins are generally discussed in a four orbital model: the two top filled and the lowest empty π-orbitals.[29] While the latter are degenerate in metalated porphyrins this degeneracy is lifted in the free base porphyrin studied here. Configuration interaction between the four possible excited configurations leads to a pair of states, absorbing around 400 nm (the B_x and B_y or Soret bands), and a pair of states Q_x and Q_y absorbing around 600 nm. While the Soret bands have a very large oscillator strength leading to a molar extinction coefficient about 10^5 $M^{-1}cm^{-1}$, that of the Q bands is at least one order of magnitude lower. While the B_x and Q_x bands are polarized along the NH – NH axis the Q_y and Q_y bands are polarized perpendicular to this axis. The splitting of B_x and B_y is often too small to observe two different bands. For Q_x and Q_y generally the two lowest vibronic bands 0-0 and 0-1 are observed.

Although no reliable absorption spectra could be obtained for the TCPP:hBN samples, fluorescence emission and excitation spectra could be obtained. Stationary emission and excitation spectra were taken for TCPP:hBN with different concentrations of the initial TCPP solution in ethanol (hence the hBN coverage level). For the emission spectra, the excitation wavelength was set to 400 nm, 440 nm, 532 nm, 550 nm, and 560 nm. We will first discuss in more detail the data obtained for the sample prepared from the TCPP solution with the lowest concentration (15 µM). This concentration is close to the one used by Korolkov *et al.*[8] (13 µM) and corresponds, using Eq. 5, and the value found for K_{LA} to a coverage of 27 %. For this sample a redshift of 610 cm^{-1} and 450 cm^{-1} is observed for respectively the $Q_x(0,0)$ and $Q_x(0,1)$ bands (see Figure 6, Figure S1 B and C, Table 2) compared to ethanol. The shift of the $Q_x(0,0)$ band is close to that observed by Korolkov *et al.*[8] for adsorption of TCPP from an 13 µM ethanol solution (680 cm^{-1}). Although the two vibronic bands observed in solution[30-33] can still

be discerned, the $Q_x(0,0)$ band is broadened from 440 cm^{-1} (width at 2/3 of the maximum) for the TCPP solution in ethanol to 870 cm^{-1} for the absorbed TCPP sample (excitation at 400 nm) (Figure 6 and Figure S1 B and C). A similar broadening is observed for other excitation wavelengths. In analogy to the solution spectra the $Q_x(0,0)$ band remains more intense than the $Q_x(0,1)$ band under all conditions The excitation spectrum recorded for the 680 nm emission, *i.e.* at the maximum of the emission, also shows a red shift of the Soret band and of the 514 nm band of the Q-band complex of respectively 830 cm^{-1} and 480 cm^{-1} (Figure 7). For the other Q-bands the signal to noise ratio did not allow to determine the position of the maximum adequately. The width (at 2/3 of the maximum) of the Soret band in the excitation spectrum of the emission at 680 nm is increased from 540 cm^{-1} for TCPP in ethanol to 1350 cm^{-1} for the adsorbed sample (excitation spectrum of the emission at 680 nm). The observation that nearly similar shifts were found for excitation and emission spectra agrees with the conclusions of Korolkov *et al.*[8] who attributed the redshift of the emission to a geometrical deformation (bowing and planarization of the phenyl rings) and to the interaction with the hBN surface, the geometrical deformation being the most important one. The geometrical distortion and the resulting electron-phonon coupling with low frequency bending vibrations of the porphyrin core could also explain the broadening of the $Q_x(0,0)$ and $Q_x(0,1)$ emission bands and of the Soret band in the excitation spectrum of the 680 nm emission. When looking at the excitation spectra (Figure 7) collected for emission between 680 nm and 640 nm, *i.e.* in the blue rising edge of the emission spectrum, we observe that upon decreasing the emission wavelength the maximum related to the Soret band gradually shifts from 432 nm to 419 nm (*i.e.* over 710 cm^{-1}), which is very close to the solution maximum (417 nm in ethanol, see SI). Also for the bluest transition of the Q-band we observe a gradual shift from 527 nm for the 680 nm emission to 517 nm (*i.e.* close to the absorption maximum at 514 nm in ethanol solution, see SI) for the 640 nm emission (*i.e.* a shift over 340 cm^{-1}). This indicates that on the blue side the broadening of the emission spectrum is partly due to the presence of a second species that undergoes both for absorption and emission, none or at least a very small redshift upon adsorption to hBN. Figure 7 A also shows that the excitation spectrum of the emission at 640

and 650 nm is narrower than that of the emission at the maximum (680 nm). The spectral features of this short wavelength species apparently correspond to those of TCPP adsorbed on TiO_2 where the $Q_x(0,0)$ and $Q_x(0,1)$ band of the emission spectrum are situated at respectively 652 nm and 719 nm, *i.e.* close to the position of those bands in ethanol solution. Finally, the excitation spectrum of the emission at 710 nm is broadened and seems a combination of the short (419 nm) and long (432 nm) wavelength band. This is related to the observation that while the emission spectrum of the long wavelength species has a minimum around 710 nm the short wavelength species, which has $Q_x(0\text{-}0)$ transition in the range 650 – 660 nm, will have a $Q_x(0\text{-}1)$ band maximum around 710 – 720 nm. As, whatever excitation wavelength chosen, the emission intensity at 640 nm is never more than 5 % of the intensity at the maximum this species must have a low abundance.

Considering the DFT calculations performed by Korolkov[8] it is not likely that the species absorbing and emitting at short wavelengths and those absorbing and emitting at long wavelengths are respectively isolated and aggregated TCPP molecules. Due to the small oscillator strength of the Q-band and the large center to center distance between flat on adsorbed TCPP molecules resonant and non-resonant interactions between neighboring TCPP molecules in the aggregates could only lead to minor shifts (respectively 2×10^{-3} eV or 16 cm^{-1} and < 10^{-3} eV or 8 cm^{-1})[8] of the spectra. Therefore, it is more probable that the short wavelength species are TCPP molecules, which are not distorted and/or interacting with the hBN surface. The photophysics of TCPP absorbed on hBN will be further explored by recording and analyzing the fluorescence decays as function of the emission wavelength and concentration of the solution from which adsorption occurred.

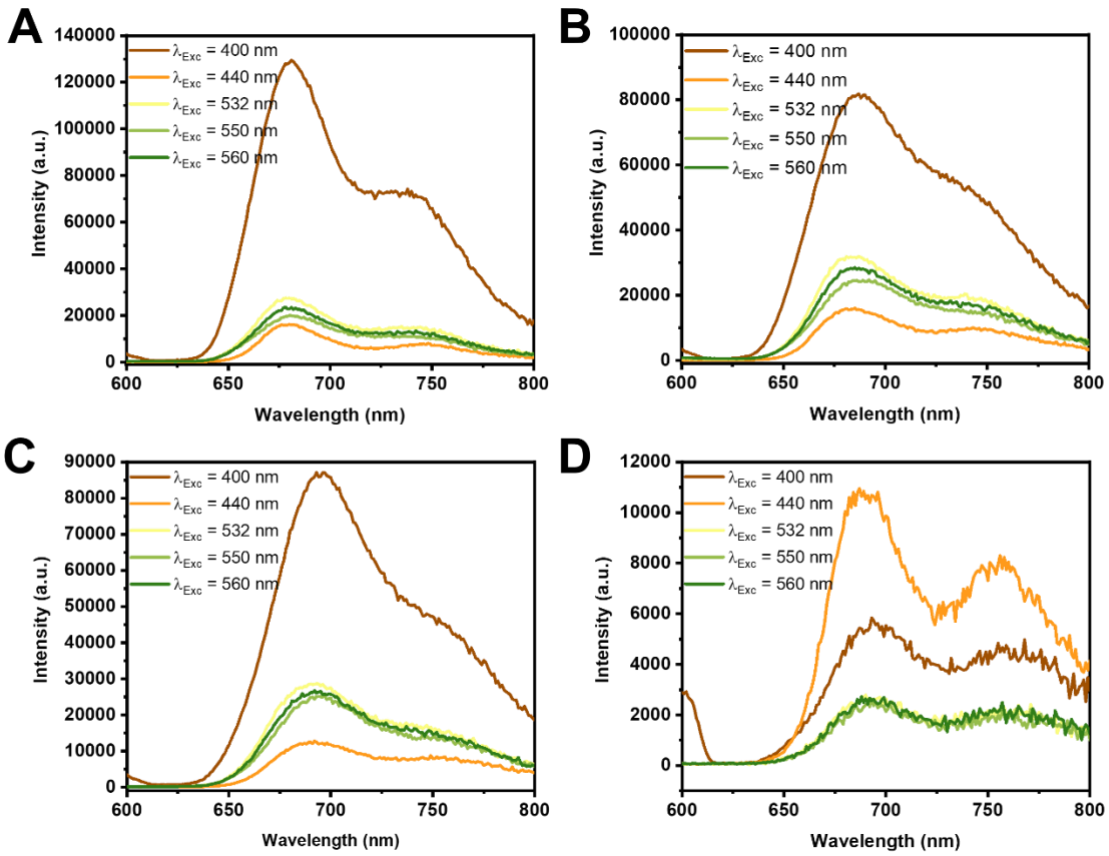

Figure 6 Emission spectrum of TCPP adsorbed on hBN from an initial solution of 15 µM (A), 75 µM (B), 150 µM (C) and 450 µM (D). The excitation wavelength was set at 400 nm, 440 nm, 532 nm, 550 nm, and 560 nm.

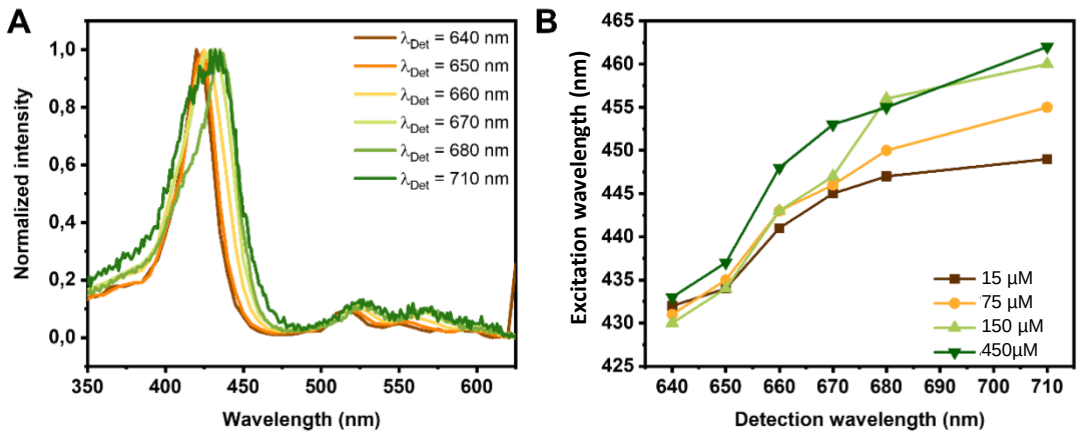

Figure 7 (A) Excitation spectrum of TCPP adsorbed on hBN from an initial solution of 15 µM. (B) Trend for the redshift of the maximum of the excitation spectrum upon increasing the coverage level by plotting the wavelength at half height (on the red side of the excitation spectra) versus the detection wavelength for concentrations 15 µM, 75 µM, 150 µM and 450 µM.

Table 2: Emission maxima of the $Q_x(0\text{-}0)$ and $Q_x(0\text{-}1)$ band of TCPP adsorbed from an initial solution in ethanol on the surface of hBN.

			Concentration			
λ_{Exc}	$Q_x(0\text{-}0)$	$\lambda_{Em,max}$	15 µM	75 µM	150 µM	450 µM
	400 nm		681	687	697	696
	440 nm		680	685	695	694
	532 nm		678	686	695	695
	550 nm		681	681	695	695
	560 nm		680	685	696	695
			Concentration			
λ_{Exc}	$Q_x(0\text{-}1)$	$\lambda_{Em,max}$	15 µM	75 µM	150 µM	450 µM
	400 nm		737	745	753	755
	440 nm		747	746	757	763
	532 nm		741	745	753	764
	550 nm		742	745	752	764
	560 nm		741	745	753	764

The fluorescence decay time of TCPP ethanol amounts to 10.21 ns (see Figure S7) which is close to the value reported for TCPP in water at pH 10 (11.3 ns).[34] For all samples of TCPP adsorbed to hBN the fluorescence decays were obtained at 653 nm, 680 nm, 717 nm and 745 nm (Figure 8), while the excitation occurred at 400 nm, *i.e.* slightly biasing the excitation to the non-interacting TCPP molecules. Although all decays are clearly non mono-exponential they start to approach an exponential decay with a similar slope at longer times. For the sample prepared from the 15 µM solution (Figure 8 A) the initial decay of the emission at 653 nm is clearly faster than that of the emission recorded at 680 and 717 nm while the decay recorded 745 nm is intermediate between the decays recorded at 653 nm and those recorded 680 nm or 717 nm. All decays of this sample could be analyzed globally, linking all decay times, as a sum of four exponentially decaying terms with decay times ranging from 0.08 to 5.93 ns (Table 3). The component with decay time τ_3 (Table 3) delivers the largest contribution to the stationary emission spectra, while τ_1 only gives a small contribution. Although the normalized amplitude (α_4) of the component with the longest decay time (τ_4) is small, it has a significant contribution to the stationary emission spectra (Table S2). Between 680 nm, 717 nm, and 745 nm, where the emission is mainly due to the long wavelength species, the amplitudes of the 0.08 ns, 0.42 ns and 1.86 ns components do not change significantly. However the

379 contribution of the 5.93 ns component is slightly smaller at 745 nm. The longest decay time of
380 5.93 ns (Table 3) can therefore be attributed to unquenched adsorbed molecules (long
381 wavelength species). This decay time is about 40 % smaller than the fluorescence decay time
382 of TCPP in ethanol solution. This could be related to the geometric distortion upon adsorption
383 leading to stronger electron phonon coupling with low frequency vibrations which is suggested
384 by the increased width of the vibronic bands (*cfr. supra*). This increased electron phonon
385 coupling leads to an increase of the Franck Condon factor for the internal conversion
386 enhancing in this way the non-radiative decay.[35,36] The faster decaying components are
387 probably due to molecules quenched by energy transfer to non-fluorescent traps, which has
388 also been observed for cyanine dyes in self-assembled films[37-39], cyanine dyes incorporated
389 in Langmuir Blodgett films[40-42] or adsorbed on hBN[13,14], and for xanthene dyes adsorbed to
390 glass or organic crystals.[43-45]

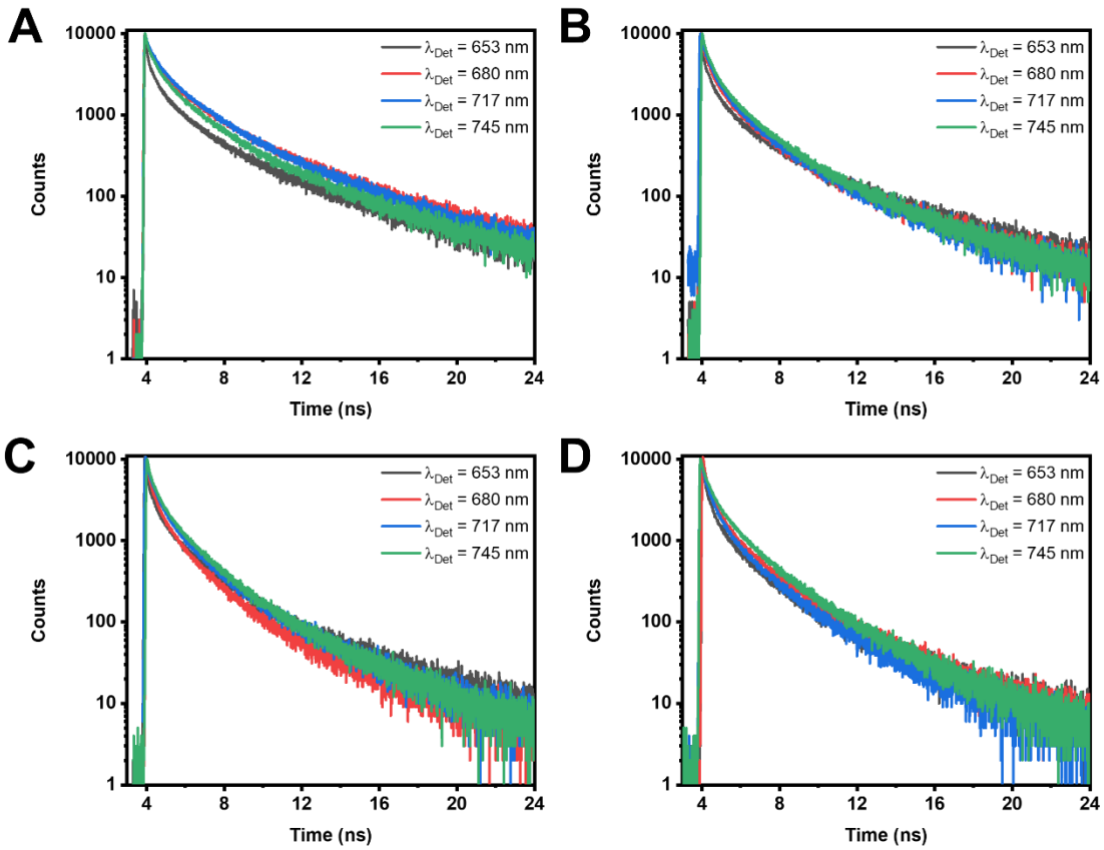

Figure 8 Fluorescence decays of TCPP adsorbed on hBN. Excitation occurred at 400 nm and the decays of the emission were recorded at 653 nm, 680 nm, 717 nm, and 745 nm. Adsorption occurred from a (A) 15 µM solution, (B) 75 µM solution, (C) 150 µM solution and (D) 450 µM solution.

In this case the fluorescence decay would be a stretched exponential rather than a sum of exponentials. However, one should note that stretched exponential decays can often be analyzed as multi-exponential decays and vice versa.[14,23] For TCPP adsorbed on hBN the presence of at least two different emitting species will further complicate the decays which for this reason were not analyzed as a stretched exponential. In spite of this ambiguity the long decay time which contributes nearly 35 % to the stationary emission (Table S2) still remains relevant as all decays become exponential at long times (Figure 8 A). When traps are present, it cannot be excluded that this long decay time can also be affected to energy hopping between neighboring TCPP molecules followed by energy transfer to the traps.[46,47]

For the emission at 653 nm, i.e. in the rising edge of the emission spectrum (Figure 6 A), α_1, the amplitude of the component with the shortest decay time (Table 3) is twice the value it has

406 at longer wavelengths leading to an overall faster decay of the fluorescence at 653 nm, which
407 can also be observed in the features of the fluorescence decays (Figure 8 A). This is also
408 reflected in the average fluorescence decay time $<\tau>$, which decreases from 0.8 – 1.0 ns at
409 longer wavelengths to 0.53 ns for the emission at 653 nm. As there is no reason why the
410 species emitting at shorter wavelengths, which is probably less distorted, should show a
411 slower radiative or non-radiative (by internal conversion or intersystem crossing) decay, the
412 faster decay of the emission at 653 nm is probably due to energy transfer to the species
413 emitting at longer wavelengths. Such exciton diffusion to species emitting at longer
414 wavelengths has been observed for *e.g.* films of poly-(3-hexyl)-thiophene,[48,49] thin films of
415 anthracene[50], or aggregates of thiacarbocyanine dyes.[51] As energy transfer only happens over
416 distances up to a few nm,[52,53] this means that the short and long wavelength species are mixed
417 on a scale of only a few nm.

418 Table 3: Decay parameters (normalized amplitudes, α_1 and decay times, τ_i) recovered from global fitting of the
419 fluorescence decays of TCPP adsorbed on hBN. Excitation occurred at 400 nm.

C (μM)	λ_{Det} (nm)	α_1 (%)	τ_1 (ns)	α_2 (%)	τ_2 (ns)	α_3 (%)	τ_3 (ns)	α_4 (%)	τ_4 (ns)	χ^2	$\langle\tau\rangle$ (ns)
15	653	64.5	0.08	21.1	0.42	11.3	1.86	3.1	5.93	1.19	0.53
	680	36.3		33.6		24.0		6.1		1.01	0.98
	717	31.8		35.4		27.4		5.5		1.05	1.01
	745	38.9		35.5		21.7		3.8		1.02	0.81
75	653	60.2	0.12	24.9	0.54	11.4	1.92	3.5	5.96	1.18	0.63
	680	50.3		32.0		15.2		2.5		1.09	0.67
	717	43.8		37.8		16.3		2.1		1.16	0.70
	745	46.6		32.7		18.3		2.4		1.05	0.73
150	653	71.0	0.07	17.8	0.36	9.1	1.53	2.1	4.63	1.20	0.35
	680	53.4		30.3		14.9		1.4		1.17	0.44
	717	35.9		43.8		18.1		2.2		1.15	0.56
	745	41.9		34.6		21.9		2.3		1.26	0.59
450	653	65.2	0.09	21.1	0.38	11.8	1.52	1.9	4.92	1.11	0.41
	680	48.7		34.2		13.7		3.4	4.02	1.17	0.52
	717	30.2		50.6		16.6		2.7		1.20	0.58
	745	27.7		43.4		25.0		3.9		1.16	0.73

420

Spectroscopy of TCPP adsorbed on hBN from more concentrated solutions

Upon increasing the concentration of the TCPP solution from which absorption occurs a further redshift of the emission maximum attributed to the $Q_x(0,0)$ and $Q_X(0,1)$ transitions, is observed (Figure 6, Table 2). This redshift is the similar for all excitation wavelengths used and amounts for the $Q_x(0,0)$ band (compared to sample prepared from the 15 µM solution) to respectively 100 ± 30 cm^{-1} for the sample prepared from the 75 µM solution and 330 ± 30 cm^{-1} for the samples prepared from the 150 µM and 450 µM solutions. Also the $Q_x(0,1)$ shows a further red shift. As except for the sample prepared form the 450 µM solution this increased redshift is accompanied by a further loss of vibronic features it is difficult to give a quantitative estimate for $Q_x(0,1)$ band of the samples prepared from 75 µM and 150 µM solutions. For the sample prepared from the 450 µM solution the clearer vibrational features (Figure 6 D) allow to determine a red shift of 360 ± 30 cm^{-1} for the $Q_x(0,1)$ band. This red shift is also accompanied by an increase of the width at 2/3 of the maximum from 870 cm^{-1} for the sample prepared from a 15 µM solution to 1150 cm^{-1} for the samples prepared from the 75 µM and 150 µM solutions and 2690 cm^{-1} for the sample prepared from the 450 µM solution. In contrast to the emission spectra the excitation spectra (Figure S6) of TCPP adsorbed on hBN from the more concentrated solutions (75 µM to 450 µM) show no red shift of the maximum compared to those where TCPP is adsorbed from a 15 µM solution (Figure 7 A). However, for the emission at 670 nm, 680 nm, and 710 nm, they become broader on the red side as shown in Figure 7 B where the wavelength where the intensity has been reduced by 50 % compared to the maximum has been plotted versus the wavelength where the emission was recorded. This indicates that adsorption from more concentrated solutions leads to the formation of a species with a red shifted absorption and emission compared to the monolayers of flat-on adsorbed TCPP formed upon adsorption from a 15 µM solution.

The broader excitation spectrum and red shifted emission observed upon adsorption from more concentrated solutions could be due to increased exciton interaction. In contrast to the flat-on adsorption occurring form dilute solutions the edge-on adsorption suggested by the

AFM experiments for adsorption from more concentrated solutions allows a smaller intermolecular distance between neighboring TCPP molecules and hence a larger exciton interaction.[26-28] This increased exciton interaction compensates the blueshift related to the flattening of the porphyrin core[8] and the decreased interaction with the substrate. The broader excitation spectra observed for samples prepared by adsorption from a more concentrated solution resemble the absorption spectra observed for TCPP nanoparticles[54] or type 3 TCPP aggregates formed in acidic aqueous solution.[34] In contrast to the results obtained for an acidified aqueous solution we did not observe the strongly blue (392 nm) or red (to 460 nm) shifted species in the excitation spectra. This could be due to the very low fluorescence quantum yield of the latter species.[34] The maximum of the $Q_x(0,0)$ band of the emission spectrum of the species formed upon adsorption from the concentrated solutions (see Figure 6 or Table 2) is shifted over 20 nm (400 cm^{-1}) to longer wavelength compared to that of the type 3 aggregates observed by Khairutdinov.[34] This could be due a stronger exciton interaction as observed for aggregates of tetrakisN-methylpyridylporphyrins[55] or residual interaction with the substrate.

Also for the samples prepared by adsorption from more concentrated solutions the fluorescence decays of each sample obtained at different emission wavelengths could be analyzed globally as a quadruple decay. While for the sample prepared from the 75 µM solution the longest two decay times (which give the major contribution to the stationary emission) are similar to those found for the sample prepared from the 15 µM solution they are significantly shorter for the samples prepared from the 150 µM and 450 µM solution (Table 3). The latter is also reflected in the smaller values of the average decay time (Table 3) and the features of the fluorescence decays (Figure 8). As observed for the sample adsorbed from the 15 µM solution the emission at the shortest wavelength (653 nm) decays faster than that at longer wavelengths which is mainly reflected in a larger amplitude of the component with the shortest decay time and a smaller amplitude of the two components with intermediate decay times. As observed for the sample prepared from the 15 µM solution the component with decay

time τ_3 has the largest contribution (p_3) to the stationary emission (Table S2). In analogy to the sample prepared from the 15 µM solution the longest decay time can be considered as a lower limit of the decay time of the unquenched molecules while the components with shorter decay times are due to energy transfer to non-fluorescent traps. This suggests that in contrast to what was observed by Khairutdinov[34] the excited state decay time of the aggregated TCPP molecules is only slightly smaller than that of the non-aggregated ones. In this respect the TCPP aggregates formed upon adsorption from more concentrated solutions resemble, as already suggested by their larger red shift those formed by tetrakisN-methylpyridyl porphyrins.[55]

CONCLUSIONS

In order to investigate the scope of the conclusions of earlier work on the adsorption of positively charged or zwitterionic thiacarbocyanine dyes on hexagonal boron nitride (hBN)[13,14] the adsorption of the neutral metalfree tetra(4-carboxyphenyl) porphyrin (TCPP) from an ethanol solution on hBN was investigated as a function of the concentration of the ethanolic solution of TCPP. While for adsorption from a dilute (15 µM) solution the features of the AFM micrographs agreed with a flat-on adsorption as shown by earlier work of Korolkov *et al.*.[8] The AFM micrographs obtained using more concentrated (up to 450 µM) solutions and the saturation coverage ($1.05 \pm 0.17 \times 10^{18}$ molecules/m^2) recovered from the adsorption isotherm suggest a transition to an edge on adsorption. In this respect the behavior of TCPP resembles that of ditridecylperylene diimide adsorbed on hBN.[7] Such transition can be driven by the preference for the tightest packing upon increasing the concentration of the adsorbate in the solution.[25] The red shift of the fluorescence spectra upon adsorption from a 15 µM ethanol solution matches that observed by Korolkov[8] and is accompanied by a similar shift of the fluorescence excitation spectrum. The latter supports the conclusion of Korolkov[8] that the red shift is due to geometrical deformation (bowing and planarization of the phenyl rings) and to the interaction with the hBN surface rather than to exciton interaction. The fluorescence and

fluorescence excitation spectra suggest also the presence of a small fraction of TCPP molecules for which this red shift is less outspoken or even absent. The fluorescence decays of TCPP adsorbed from a 15 µM solution are non mono-exponential which in analogy with cyanine dyes adsorbed on hBN,[13,14] incorporated in Langmuir Blodgett films,[40-42] or in self-assembled films,[37-39] and for xanthene dyes adsorbed to glass or organic crystals[43-45] was attributed to quenching by energy transfer to non-fluorescent traps. At long times, all decays become exponential with a decay time which is for the sample prepared using the 15 µM solution 40 % shorter than the fluorescence decay time in ethanol. This shorter decay time can be related[35,36] to the bowing of the porphyrin rings[8] upon adsorption although exciton diffusion to non-fluorescent traps cannot be excluded completely.[46,47]

Upon increasing the concentration of the initial TCPP solution from which adsorption occurs, a red shift and broadening of the emission spectrum is accompanied by a broadening of the fluorescence excitation spectrum. This is attributed to interaction between neighboring chromophores as the edge on orientation of the adsorbed TCPP molecules at higher concentration of the initial solution allows a cofacial packing of neighboring chromophores. For this cofacial packing the smaller intermolecular distance will allow a stronger interaction between neighboring chromophores than allowed by the lateral interaction of flat-on adsorbed TCPP molecules. While the features of the excitation spectrum of these TCPP aggregates resemble those of TCPP aggregates formed in acidified water or TCPP nanoparticles[34,54] their emission spectrum is red shifted and the fluorescence decay time is an order of magnitude larger compared to the aggregates formed in aqueous solution resembling in this way aggregates of tetrakis N-methylpyridylporphyrins.[55]

Acknowledgments

The authors are thankful for the support from the Research Council of KU Leuven through the project C14/19/079 (FUEPONA), the Research Foundation Flanders (FWO) through the projects G0F8217N and G082215N, and a fellowship to J.VdW (11F3520N). SFLM acknowledges support from the Austrian Science Fund (FWF, project I3256-N36) and Material Science Institute (Lancaster University) international funds. The authors want to thank prof. Kenji Watanabe and prof. Takashi Taniguchi of the National Institute for Material Science (NIMS), Tsukuba, Japan for a gift of hBN crystals.

Appendix A.

Supplementary data Supplementary data to this article can be found online at xxx

References

1. Wang, H., Zhao, Y., Xie, Y., Ma, X., Zhang, X. Recent progress in synthesis of two-dimensional hexagonal boron nitride. *J. Semicond.* **38**, 031003 (2017).
2. Weng, Q., Wang, X., Wang, X., Bando, Y., Golberg, D. Functionalized hexagonal boron nitride nanomaterials: emerging properties and applications. *Chem. Soc. Rev.* **45**, 3989–4012 (2016).
3. Cassabois G., Valvin, P., Gil, B., Hexagonal boron nitride is an indirect bandgap semiconductor, *Nat. Photonics* **10** 262-266 (2016).
4. Elias, C., Valvin, P., Pelini, T., Summerfield, A., Mellor, C.J., Cheng, T.S., Eaves, L., Foxon, C.T., Beton, P.H., Novikov, S.V., Gil, B., Cassabois, G., Direct band-gap crossover in epitaxial monolayer boron nitride, *Nat. Commun.* **10**, 2639 (2019).
5. Forster, M., Parker, J.E., Inaba, A., Murray, C.A., Strange, N.A., Larese, J.Z., Arnold, T. The Mixing Behavior of Alkanes Adsorbed on Hexagonal Boron Nitride. *J. Phys. Chem. C* **120**, 25796–25805 (2016).
6. Arnold, T., Parker, J. E., Macdonald, P. Investigation of the Adsorption of Alkanes on Hexagonal Boron Nitride from Their Liquids and Binary Mixtures. *J. Phys. Chem. C* **116**, 10599–10606 (2012).
7. Sun, B., Xu, X., Zhou, G., Tao, L., Wang, X., Xu, J.-B. Observation of Strong J -Aggregate Light Emission in Monolayer Molecular Crystal on Hexagonal Boron Nitride. *J. Phys. Chem. A* **124**, 7340–7345 (2020).
8. Korolkov, V.V., Svatek, S.A., Summerfield, A., Kerfoot, J., Yang, L., Taniguchi, T., Watanabe, K., Champness, N.R., Besley, N.A., Beton, P.H. van der Waals-Induced

Chromatic Shifts in Hydrogen-Bonded Two-Dimensional Porphyrin Arrays on Boron Nitride. *ACS Nano* **9**, 10347–10355 (2015).

9. Arnold, T., Forster, M., Fragkoulis, A. A., Parker, J. E. Structure of Normal-Alkanes Adsorbed on Hexagonal-Boron Nitride. *J. Phys. Chem. C* **118**, 2418–2428 (2014).

10. Arnold, T., Dong, C.-C., Thomas, R.K., Castro, M.A., Perdigon, A., Clarke S.M., Inaba, A. The crystalline structures of the odd alkanes pentane, heptane, nonane, undecane, tridecane and pentadecane monolayers adsorbed on graphite at submonolayer coverages and from the liquid. *Phys. Chem. Chem. Phys.* **4**, 3430–3435 (2002).

11. Arnold, T., Thomas, R.K., Castro, M.A., Clarke, S.M., Messe, L., Inaba, A. The crystalline structures of the even alkanes hexane, octane, decane, dodecane and tetradecane monolayers adsorbed on graphite at submonolayer coverages and from the liquid. *Phys. Chem. Chem. Phys.* **4**, 345–351 (2002).

12. Kruchten, F., Knorr, K., Volkmann, U.G., Taub, H., Hansen, F.Y., Matthies, B., Herwig, K.W. Ellipsometric and Neutron Diffraction Study of Pentane Physisorbed on Graphite. *Langmuir* **21**, 7507–7512 (2005).

13. Nellissen, A.-C., Steeno, R., Vandenwijngaerden, J.B.F., De Feyter, S., Mertens, S.F.L., Van der Auweraer, M. The behavior of thiacarbocyanine dyes on the surface of few-layered hexagonal boron nitride. *Dye. Pigm.* **208**, 110790 (2022).

14. Nellissen, A.-C., Fron, F., Vandenwijngaerden, J.B.F., De Feyter, S., Mertens, S.F.L., Van der Auweraer, M. Spectroscopic Characterization of Thiacarbocyanine Dye Molecules Adsorbed on Hexagonal Boron Nitride: a Time-Resolved Study. *ACS Omega* **8**, 35638-35652 (2023).

15. Albar, J.D., Korolkov, V.V., Baldoni, M., Watanabe, K., Taniguchi, T., Besley, E., Beton, P.H. Adsorption of Hexacontane on Hexagonal Boron Nitride. *J. Phys. Chem. C* **122**, 27575–27581 (2018).

16. Kerfoot, J., Svatek, S.A., Korolkov, V.V., Taniguchi, T., Watanabe, K., Antolini, E., Beton, P.H. Fluorescence and Electroluminescence of J-Aggregated Polythiophene Monolayers on Hexagonal Boron Nitride. *ACS Nano* **14**, 13886–13893 (2020).

17. Cherian, S., Wamser, C. C. Adsorption and Photoactivity of Tetra(4-carboxyphenyl)porphyrin (TCPP) on Nanoparticulate TiO_2. *J. Phys. Chem. B* **104**, 3624–3629 (2000).

18. Steeno, R., Rodriguez-González, M.C., Eyley, S., Thielemans, W., Mali, K.S., De Feyter, S. Covalent Functionalization of Carbon Surfaces: Diaryliodonium versus Aryldiazonium Chemistry. *Chem. Mater.* **32**, 5246–5255 (2020).

19. Maus M, Rousseau E., Cotlet M, Schweitzer G, Hofkens J, Van der Auweraer M, De Schryver F C, Krueger A. New picosecond laser system for easy tunability over the whole ultraviolet/visible/near infrared wavelength range based on flexible harmonic generation and optical parametric oscillation. *Rev. Sci. Instrum.* **72**, 36–40 (2001).

20. Boens, N. , Qin, W., Basarić, N., Hofkens, J., Ameloot, M., Pouget, J., Lefèvre, J.-P., Valeur, B., Gratton, E., van de Ven, M., Silva, N.D., Engelborghs, Y., Willaert, K., Sillen, A., Rumbles, G., Phillips, D., van Hoek, A., Lakowicz, J.R., Malak, H., Gryczinski, I., Szabo, A.G., Krajcarski, D.T., Tamai, N., Miura, A. Fluorescence Lifetime Standards for Time and Frequency Domain Fluorescence Spectroscopy. *Anal. Chem.* **79**, 2137–2149 (2007).

21. Lakowicz, J. R. *Principles of Fluorescence Spectroscopy*. (Springer US, 2006).

22, Baekelant, W., Aghakhani, S., Coutino-Gonzalez, E., Grandjean, D., Kennes, K., Jonckheere, D., Fron, E., d'Acapito, F., Longo, A., Lievens, P., Roeffaers, M.B.J.,

606 Hofkens, J. Confinement of Highly Luminescent Lead Clusters in Zeolite A. *J. Phys.*
607 *Chem. C* **122**, 13953–13961 (2018).

608 23. Van der Auweraer, M., Ballet, P., De Schryver, F. C., Kowalczyk, A. Parameter recovery
609 and discrimination between different types of fluorescence decays obtained for dipole-
610 dipole energy transfer in low-dimensional systems. *Chem. Phys.* **187**, 399–416 (1994).

611 24. Atkins, P., de Paula, J. *Atkins' Physical chemistry*. *Atkins' Physical chemistry* (Oxford
612 University Press, (2014).

613 25. Lei, S., Tahara, K., De Schryver, F.C., Van der Auweraer, M., Tobe, Y., De Feyter, S.,
614 One Building Block, Two Different Supramolecular Surface-Confined Patterns:
615 Concentration in Control at the Solid/liquid Interface. *Angew. Chem*. **47**, 2964-2968
616 (2008).

617 26. Kasha, M. Energy Transfer Mechanisms and the Molecular Exciton Model for Molecular
618 Aggregates. *Radiat. Res.* **20**, 55-71 (1963).

619 27. Förster, T. Delocalization excitation and excitation transfer. in *Modern Quantum*
620 *Chemistry* Vol. ,**3B,** Ed. O.,Sinanoglu, 93–137, Academic Press, New York (1965).

621 28. Deshmukh, A.P., Geue, N., Bradbury, N.C., Atallah, T.L., Chuang, C., Pengshung, M.,
622 Cao, J., Sletten, E.M.. Bridging the gap between H- and J-aggregates: Classification
623 and supramolecular tunability for excitonic band structures in two-dimensional
624 molecular aggregates. *Chem. Phys. Rev.* **3**, 021401 (2022).

625 29 Gouterman M., Spectra of Porphyrins, *J. Mol. Spectr.*, **6**, 138-163 (1961).

626 30. Lewandowska, K., Rosiak, N., Bogucki, A., Cielecka-Piontek, J., Mizera, M., Bednarski,
627 W., Suchecki, M., Szaciłowski, K.. Supramolecular Complexes of Graphene Oxide with
628 Porphyrins: An Interplay between Electronic and Magnetic Properties, *Molecules*, **24**,
629 688-707 (2019).

630 31. Castriciano, M.A., Romeo, A., Angelini, N., Micali, N., Longo, A., Mazzaglia. A.,
631 Monsu'Scolaro L.. Structural Features of meso-Tetrakis(4-carboxyphenyl)porphyrin
632 Interacting with Amino-Terminated Poly(propylene oxide). *Macromolecules*, **39**, 5489-
633 5496 (2006).

634 32. Weinkauf, J.R., Cooper, S.W., Aaron Schweiger, A., Wamser C.C.. Substituent and
635 Solvent Effects on the Hyperporphyrin Spectra of Diprotonated Tetraphenylporphyrins.
636 J*. Phys. Chem. A*, **107**, 3486-3496 (2003).

637 33. Fonda, H.N., Gilbert, J.V., Cormier, R.A., Sprague, J.R., Kamioka, K., Connolly, J.S.,
638 Spectroscopic, photophysical, and redox properties of some meso-substituted free-
639 base porphyrins, *J. Phys. Chem.*, **97**, 7024–7033 (1993).

640 34. Khairutdinov, R.F., Serpone, N. Photoluminescence and Transient Spectroscopy of
641 Free Base Porphyrin Aggregates. *J. Phys. Chem. B***, 103***,* 761-769 (1999).

642 35. Jiao, L., Yu, C., J. Wang, J., Briggs, E.A., Besley, N.A., Robinson, D., Ruedas-Rama,
643 M.J., Orte, A., Crovetto, L., Talavera, E.M., Alvarez-Pez, J.M., Van der Auweraer, M.,
644 Boens, N., Unusual spectroscopic and photophysical properties of *meso-tert*-butylBODIPY
645 in comparison to related alkylated BODIPY dyes. *RSC Adv.* **5**, 89375 (2015).

646 36. Zha, M., Lin, X., Ni, J.-S., Li, Y., Zhang, Y., Zhang, X., Wang, L., Li, K. An Ester-
647 Substituted Semiconducting Polymer with Efficient Nonradiative Decay Enhances NIR-
648 II Photoacoustic Performance for Monitoring of Tumor Growth. *Angew. Chem. Int. Ed.*
649 **59**, 23268–23276 (2020).

650 37. Rousseau, E., Van Der Auweraer, M., De Schryver, F. C. Steady-state and time-
651 resolved spectroscopy of a self-assembled cyanine dye multilayer. *Langmuir* **16**, 8865–
652 8870 (2000).

653 38. Kometani, N., Nakajima, H., Asami, K., Yonezawa, Y., Kajimoto, O. Excited-state
654 dynamics of the mixed J-aggregate of two kinds of cyanine dyes in layer-by-layer
655 alternate assemblies. *Chem. Phys. Lett.* **294**, 619–624 (1998).

656 39. Kometani, N., Nakajima, H., Asami, K., Yonezawa, Y., Kajimoto, O. Luminescence
657 Properties of the Mixed J-Aggregate of Two Kinds of Cyanine Dyes in Layer-by-Layer
658 Alternate Assemblies. *J. Phys. Chem. B* **104**, 9630–9637 (2000).

659 40. Ballet, P., Van der Auweraer, M., De Schryver, F. C., Lemmetyinen, H. & Vuorimaa, E.
660 Global Analysis of the Fluorescence Decays of N,N'-Dioctadecyl Rhodamine B in
661 Langmuir−Blodgett Films of Diacylphosphatidic Acids. *J. Phys. Chem.* **100**, 13701–
662 13715 (1996).

663 41. Laguitton Pasquier, H., Pevenage, D., Ballet, P., Vuorimaa, E., Lemmetyinen, H.,
664 Jeuris, K., De Schryver, F.C., Van der Auweraer, M. Space and Time Resolved
665 Spectroscopy of Two-Dimensional Molecular Assemblies. in Valeur, B. & Brochon, J.-
666 C.Eds., *New Trends in Fluorescence Spectroscopy, Springer Series on Fluorescence*
667 ***vo*l 1**, 99-124 (Springer Berlin Heidelberg, 2001).

668 42. Pevenage, D., Van der Auweraer, M., De Schryver, F. C. Influence of the Molecular
669 Structure on the Lateral Distribution of Xanthene Dyes in Langmuir−Blodgett Films.
670 *Langmuir* **15**, 8465–8473 (1999).

671 43. Willig, F., Blumen, A., Zumofen, G. Dynamics of fluorescence quenching in disordered
672 dye monolayers. *Chem. Phys. Lett.* **108**, 222–227 (1984).

673 44. Kemnitz, K., Murao, T., Yamazaki, I., Nakashima, N., Yoshihara, K. Picosecond
674 fluorescence measurement of submono- and mono-layer of adsorbed rhodamine B on
675 a single crystal of naphthalene and on glass. *Chem. Phys. Lett.* **101**, 337–340 (1983).

676 45. Nakashima, N., Yoshihara, K., Willig, F. Time-resolved measurements of electron and
677 energy transfer of rhodamine B monolayer on the surface of organic crystals. *J. Chem.*
678 *Phys.* **73**, 3553–3559 (1980).

679 46. Zumofen, G., Blumen, A. Random-walk studies of excitation trapping in crystals. *Chem.*
680 *Phys. Lett.* **88**, 63–67 (1982).

681 47. Pandey, L., Van der Auweraer, M. Energy transfer dynamics in organic light emitting
682 diode emission layers doped with triplet emitters. *J. Appl. Phys.* **110**, 053712 (2011).

683 48. Masri, Z., Ruseckas, A., Emelianova, E.V., Wang, L., Bansai A.K., Matheson, A.,
684 Nielsen, M.M., Nguyen, H., Coulembier, O., Dubois, P., Beljonne, D., Samuel, D.W.
685 Molecular Weight Dependence of Exciton Diffusion in Poly(3-hexylthiophene). *Adv.*
686 *Energy Mater.* **3**, 1445–1453 (2013).

687 49. Ghosh, R., Spano, F. C. Excitons and Polarons in Organic Materials. *Acc. Chem. Res.*
688 **53**, 2201–2211 (2020).

689 50. Ahn, T.-S., Müller, A.M., Al-Kaysi, R.O., Spano, F.C., Noeton, J.E., Beljonne, D.,
690 Brédas, J.-L., Bardeen, C.. Experimental and theoretical study of temperature
691 dependent exiton delocalization and relaxation in anthracene thin films. *J. Chem. Phys.*
692 **128**, 054505 (2008).

693 51. Scheblykin, I. G., Sliusarenko, O. Y., Lepnev, L. S., Vitukhnovsky, A. G. & Van der
694 Auweraer, M. Excitons in Molecular Aggregates of 3,3'-Bis-[3-sulfopropyl]-5,5'-dichloro-
695 9-ethylthiacarbocyanine (THIATS): Temperature Dependent Properties. *J. Phys.*
696 *Chem. B* **105**, 4636–4646 (2001).

697 52. Th, Förster, Th. Zwischenmolekulare Energiewanderung und Fluorezenz, *Annalen der*
698 *Physik*, **6** 55-7. (1948).

699 53. Agranovich, V.D., Galanin, M.D. Electronic excitation energy transfer in condensed
700 matter. North-Holland Publishing Company (1982).

54. Wu, Q., Xia, R., Li, C., Li, Y., Sun, T., Xie, Z., Jing, X.. Nanoscale aggregates of porphyrins: red-shifted absorption, enhanced absorbance and phototherapeutic activity. *Mater. Chem. Front.***, 5**, 8333-8340 (2021).

55. Vergeldt, J.J., Koehorst, R.B.M., van Hoek, A., Schaafsma, T.J.. Intramolecular interactions in the ground and excited states of tetrakis (N-methylpyridyl) porphyrins, *J. Phys. Chem.*, **99**, 4397-4405 (1995).